Patient-Specific Hemodynamic Evaluation of an Aortic Coarctation under Rest and Stress Conditions

Priti G. Albal[1,4], Tyson A. Montidoro[2], Onur Dur[3], and Prahlad G. Menon[1,4,5]

[1] Yat-sen University - Carnegie Mellon University (SYSU-CMU)
Joint Institute of Engineering (JIE), Pittsburgh, PA, USA
[2] Department of Biomedical Engineering, Carnegie Mellon University, Pittsburgh, PA, USA
[3] Thoratec Corporation, Pleasanton, CA, USA
[4] QuantMD LLC, Pittsburgh, PA, USA
[5] SYSU-CMU, Shunde International Joint Research Institute, Guangdong, China
pgmenon@andrew.cmu.edu

Abstract. Computational fluid dynamics (CFD) simulation of internal hemodynamics in complex vascular models can provide accurate estimates of pressure gradients to assist time-critical diagnostics or surgical decisions. Compared to high-fidelity pressure transducers, CFD offers flexibility to analyze baseline hemodynamic characteristics at rest but also under stress conditions without application of pharmacological stress agents which present undesirable side effects. In this study, the variations of pressure gradient and velocity field across a mild thoracic coarctation of aorta (CoA) is studied under pulsatile ascending aortic flow, simulative of both rest and stress cardiac output. Simulations were conducted in FLUENT 14.5 (ANSYS Inc., Canonsburg, PA, USA) - a finite volume solver, COMSOL 4.2a (COMSOL Multiphysics Inc., Burlington, MA) - a finite element solver, and an in-house finite difference cardiovascular flow solver implementing an unsteady artificial compressibility numerical method, each employing second-order spatio-temporal discretization schemes, under assumptions of incompressible, Newtonian fluid domain with rigid, impermeable walls. The cardiac cycle-average pressure drop across the CoA modeled relative to the given pressure data proximal to the CoA is reported and was found to vary significantly between rest and stress conditions. A mean pressure gradient of 2.79 mmHg was observed for the rest case as compared to 17.73 mmHg for the stress case. There was an inter-solver variability of 16.9% in reported mean pressure gradient under rest conditions and 23.71% in reported mean pressure gradient under stress conditions. In order to investigate the effects of the rigid wall assumption, additional simulations were conducted using a 3-element windkessel model implemented at the descending aorta, using FLUENT. Further, to investigate the appropriateness of the inviscid flow assumption in a mild CoA, CFD pressure gradients were also compared results of a simple Bernoulli-based formula, used clinically, using just the peak blood flow velocity measurements (in m/s) obtained distal to the aortic coarctation from CFD. Helicity isocontours were used as a visual metric to characterize pathological hemodynamics in the CoA.

1 Introduction

Coarctation of the aorta (CoA) is a common congenital disease present in adolescence or adulthood, and often identified in the context of investigation for hypertension

O. Camara et al. (Eds.): STACOM 2013, LNCS 8330, pp. 83–93, 2014.

[1, 2]. CoA is often associated with other congenital diseases including atrial septa defect, pulmonary stenosis, etc [3, 4]. Decrease in regional diameter at the aortic coarctation results in elevated pressure gradients across it. These pressure gradients increase several fold under stress conditions, in contrast with rest conditions[5]. Compared to high-fidelity pressure transducers employed during invasive pressure measurement, computational fluid dynamics (CFD) offers flexibility to analyze baseline pre-repair hemodynamic characteristics non-invasively at rest and also under stress conditions *in-silico*, without application of pharmacological stress agents which present undesirable side effects, including chest pain, blood pressure decrease, arrhythmia, palpitations, shortness of breath and headaches [6, 7]. CFD can provide information regarding peak velocities distal to CoA and visual representations of flow structures using flow derived parameters such as helicity isocontours which can objectify characterizing the pathological extent of pre-repair CoA hemodynamics[8]. In this study, we use CFD to predict pressure gradients across a mild CoA (~30%) in a17-year old male patient, at both rest (Re = 95) and pharmacological stress conditions (Re = 3400) [5]. We provide a comparison of results between two commercial solvers – a finite volume (FVM) and a finite element (FEM) solver – as well as one in-house finite difference (FDM) solver, each set up to model rigid-wall CFD supplied with the same inflow and outflow conditions specified for the 2013 STACOM CFD Challenge. Pressure gradients from CFD were compared against those obtained from the commonly used clinical formula [9], $\Delta P = 4V^2$, where V is the peak velocity (in m/s) distal to CoA, in order to assess the validity of the Bernoulli assumptions it is based upon (i.e. inviscid flow) in the context of a mild CoA.

The paper is organized as follows: in section 2.1, the computational methods for the three different solvers utilized in this study are described including methods for data sampling and analysis. Section 2.2 presents a mesh sensitivity analysis conducted to ensure consistency and convergence of the CFD solution. In section 2.3, the method for implementing a 3-element windkessel model at the descending aorta (DAo) is described for the purpose of analyzing transient differences in pressure gradients across the CoA between the rigid wall models and one that considers compliance. Finally, section 3 presents the pressure gradients and velocity fields at rest and stress conditions, contrasting results from the three solvers along with a discussion of the limitations of this study in section 4.

2 Methods

2.1 Inter-solver Variability – A Verification Study

The numerical solution to the Navier-Stokes (NS) equations modeling incompressible, viscous flow may be arrived at in a discretized fluid domain by using multiple established numerical methods[10-13], within an FEM, FDM or FVM discretization framework. For this study, simulations were conducted in FLUENT 14.5 (ANSYS Inc., Canonsburg, PA, USA) - a FVM solver, COMSOL 4.2a (COMSOL Multiphysics Inc., Burlington, MA) – FEM solver and an in-house FDM cardiovascular flow solver implementing an unsteady artificial compressibility numerical method, each employing second-order spatio-temporal discretization schemes, under assumptions

of incompressible, Newtonian fluid domain with rigid, impermeable walls. The aorta CoA model examined in this study was segmented from a contrast enhanced magnetic resonance angiography (MRA) and was provided as a STL file for the CFD Challenge. The STL surface mesh was converted into solid model constituted of NURBS patches after conducting minimal surface correction operations and finally exported as an IGS file for purposes of universal compatibility with different solvers. Direct numerical solutions (DNS) CFD was performed without considering a turbulence model, as per the specifications of the CFD challenge, for identical rigid-wall geometry, inlet flow rates (as provided for rest and stress conditions) with a plug profile and outlet mass-flow splits. Outlet mass-flow splits of 17%, 8%, 10% and 65% were applied for the rest condition and 25%, 5%, 11% and 59% were applied for the stress condition, at the Innominate, left carotid, left subclavian and DAo branches, respectively.

Finite Volume Solver: FLUENT

FLUENT is a FVM code. The IGS geometry was meshed in ANSYS Workbench 14. The curvature-based advanced mesh size function tool was used to obtain better mesh resolution in the region of the coarctation. A mesh containing ~500,000 tetrahedral elements was considered for the final FLUENT simulations reported in this study. A mesh sensitivity analysis was also performed as described in section 2.2. A User Defined Function (UDF) was implemented to input pulsatile mass flow rate waveform at the inlet for rest and stress cases. The pressure at the inlet was set to 63.35 mmHg for rest conditions and 64.3 mmHg for stress conditions. For all the FLUENT simulations, the pressure-velocity coupling algorithm was set as SIMPLE which implements a pressure based segregated algorithm. The SIMPLE algorithm uses a relationship between velocity and pressure corrections to enforce mass conservation and to obtain the pressure field. A second-order discretization of pressure and momentum terms was employed. The pressure discretization method was set as PRESTO!, recommended for complex geometries which induce swirl flow such as the aorta model. A second-order implicit time advancement with a fixed time step of 0.016 sec was chosen.

Finite Element Solver: COMSOL

COMSOL Multiphysics is a FEM code. A mesh containing ~600,000 and ~1,000,000 tetrahedral elements with an imposed boundary layer mesh was considered for the final rest and stress case COMSOL simulations respectively. The inlet flow waveform (15 Fourier-term waveform reconstructions) was specified at the inlet via COMSOL's live-link capabilities using MATLAB 2011b (The MathWorks Inc., Natrick, MA). A constant pressure was imposed at the inlet of the model as per the given pressure waveform. Simulations were conducted using the laminar flow module and a time dependent study. Furthermore, a preconditioned generalized minimal residual method (GMRES) iterative solver for the flow field at each time step and a constant (Newton) nonlinear solver time marching were implemented. Also, to aid in convergence for a highly nonlinear problem, the Jacobean matrix was updated after every iteration.

Finite Difference Solver- In-House Solver

DNS was also performed using a second-order accurate, in-house FDM, artificial compressibility numerical solver. This solver has been used extensively for image-based hemodynamic modeling and incorporates a validated multi-grid artificial compressibility numerical solver [8, 14, 15]. Flow was simulated on a high-resolution unstructured Cartesian immersed boundary grid composed of ~500,000 uniformly spaced nodes, with an average node spacing resolution of 0.02 mm, which was generated after immersing the surface model in a Cartesian grid of 498 x 126 x 156 cubical elements. Computations were performed using normalized spatial and temporal units. The temporal resolution was considered as 0.01 simulation time units i.e. ~O (10^{-4}) sec. A second order interpolation scheme was employed in order to obtain inlet conditions based on the input discrete cardiac cycle data. Mean pressure at the inlet was set to the mean of the given pressure waveforms.

Data Sampling

For the purpose of standardizing data collection a plane proximal to CoA and plane distal to CoA were defined as specified in Table 1. All results for pressure gradient across the CoA were reported at these planes and data was gathered for the 5th cardiac cycle, in order to ensure damping of initial transients.

Table 1. Planes before and after CoA defined by a point and through through the plane

	Origin	**Normal to plane**
Proximal plane	(188.96, 40.18, 253.22)	(0.98,-0.09,-0.19)
Distal plane	(261.97,23.56,277.10)	(0.99,-0.03,-0.14)

2.2 Mesh Sensitivity Analysis

A fine mesh (Fig 1a, 1c) consisting of ~500,000 elements and a coarse mesh (Fig 1b) consisting of ~250,000 elements were considered for the mesh sensitivity study in case of FLUENT. Flow was simulated for these meshes as described in section 2.1. The differences in pressure values for the two meshes for stress case are presented in Table 2 and Fig 2. Minor changes were observed before and after the CoA as a result of increasing the mesh size in FLUENT. As the mesh was refined similar consistency was observed in the reported pressure gradients for the in-house solver. In case of COMSOL, a finer mesh was required to obtain accurate results as per mesh sensitivity convergence tests. A mesh containing ~600,000 and ~1,000,000 tetrahedral elements was considered for the final rest and stress case COMSOL simulations respectively. Even for such fine meshes, the pressure results did were only approaching convergence but mesh refinement. Since the aim of this study was to compare pressure gradients using three solvers for similar mesh sizes, the mesh wasn't refined beyond this point. The FLUENT simulation results can be considered most accurate in this study since the pressure results converged appropriately as the final mesh density was approached.

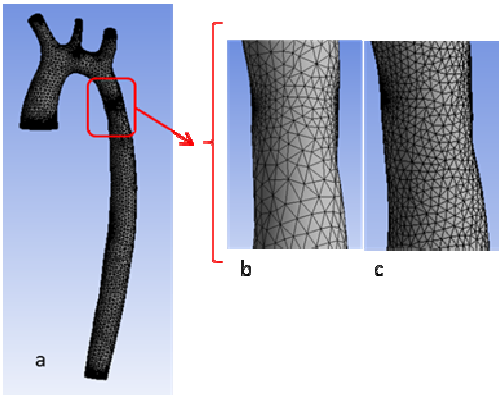

Fig. 1. a) Meshed aorta model used for the FLUENT simulation. Coarse (b), and fine (c) mesh seen at the coarctation.

Table 2. Reported area averaged pressure values at stress condition for mean flow proximal and distal to CoA for different number of mesh elements

Number of mesh elements	Area averaged pressure proximal to CoA (mmHg)	Area averaged pressure distal to CoA (mmHg)
250,000	61.075	48.275
500,000	61.15	46.83

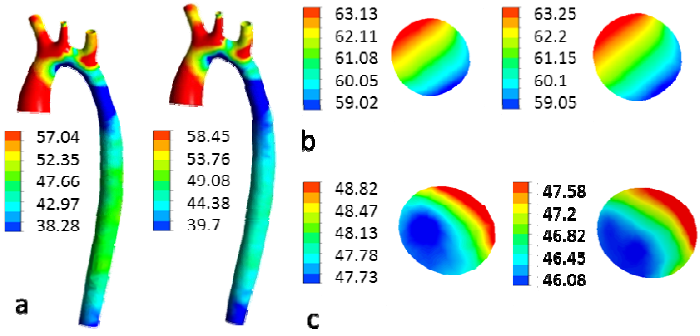

Fig. 2. Difference in pressure gradient for coarse (left) and fine (right) mesh at the walls (a), proximal plane (b) and distal plane (c), under rest-state conditions

2.3 3-Element Windkessel Modeling at DAo

The purpose of the windkessel modeling was to investigate the influence of compliance of walls on mean pressure gradients as well as its transient variation, only for the rest-state condition, in contrast with the rigid-wall CFD simulations described earlier (section 2.1) which did not factor compliance at all. In an effort to compensate

for the compliant effect of the arterial walls and thereby tune the CFD results to match physiological pressure estimates [16, 17], a viscoelastic three element Windkessel model (Fig 3) was implemented based on the following equation, at the DAo:

$$\left(1+\left(\frac{R_1}{R_2}\right)\right)Q_i + C\,R1\,\frac{dQ_i}{dt} = \frac{P_i}{R_2} + C\,\frac{dP_i}{dt} \tag{1}$$

where, R_1 is the primary resistance adjusted to yield required pressure at the baseline flow, C is compliance set such that time constant of pressure decay (R_1C) is around 2.5s. This represents the systemic arterial impedance at the downstream of the head-neck vessels and DAo. For this study, values of R_1, R_2 and C (see Fig 3) were considered as 1527mmHg-s/L, 100mmHg-s/L and 0.00164L/mmHg respectively. R_1 was tuned so as to match the given rest-state outlet mass flow splits without the compliance being factored in. Solving the linear algebraic-differential equation system on the model interface, the lumped parameter model represents the effect of the downstream domain as a semi-implicit function of pressure, which was used to couple the upstream three-dimensional numerical domain with the downstream analytic domain.

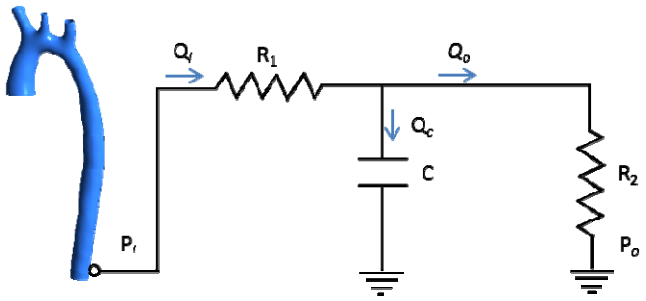

Fig. 3. Windkessel boundary condition imposed at the DAo

3 Results and Discussion

A solver-average mean pressure gradient of 2.79±0.7 mmHg was observed for the rest case as compared to 17.73±6.3 mmHg for the stress case as an average for all 3 rigid wall simulations (Table 3). An inter-solver variability of 16.9% was reported for mean pressure gradient for rest conditions and 23.7% was reported for mean pressure gradient for stress conditions. Exact flow splits were obtained at every time step for FLUENT simulations and in-house solver owing to the applied mass flow-split outflow boundary conditions. For COMSOL, computed flow splits were matched within 2.5% error for the rest case and within 1.2% for the stress. Mean flows of 10508, 4925, 6204 and 40635 mm^3/s were measured for rest case and 55732, 11146, 24522 and 131527 mm^3/s for measured for stress case through outlets one to four respectively. Renderings of the pressure field across the CoA from each of the three solvers (sections 2.1) can be seen in Fig 4. The mean pressure drop computed using Bernoulli

principle across the coarctation using the mean CFD velocities observed in the plane distal to the CoA was ~18mmHg for rest conditions and ~90mmHg for stress conditions at peak flows which was an overestimation (~2 times higher) as compared to the pressure field reported from rigid wall CFD simulations.

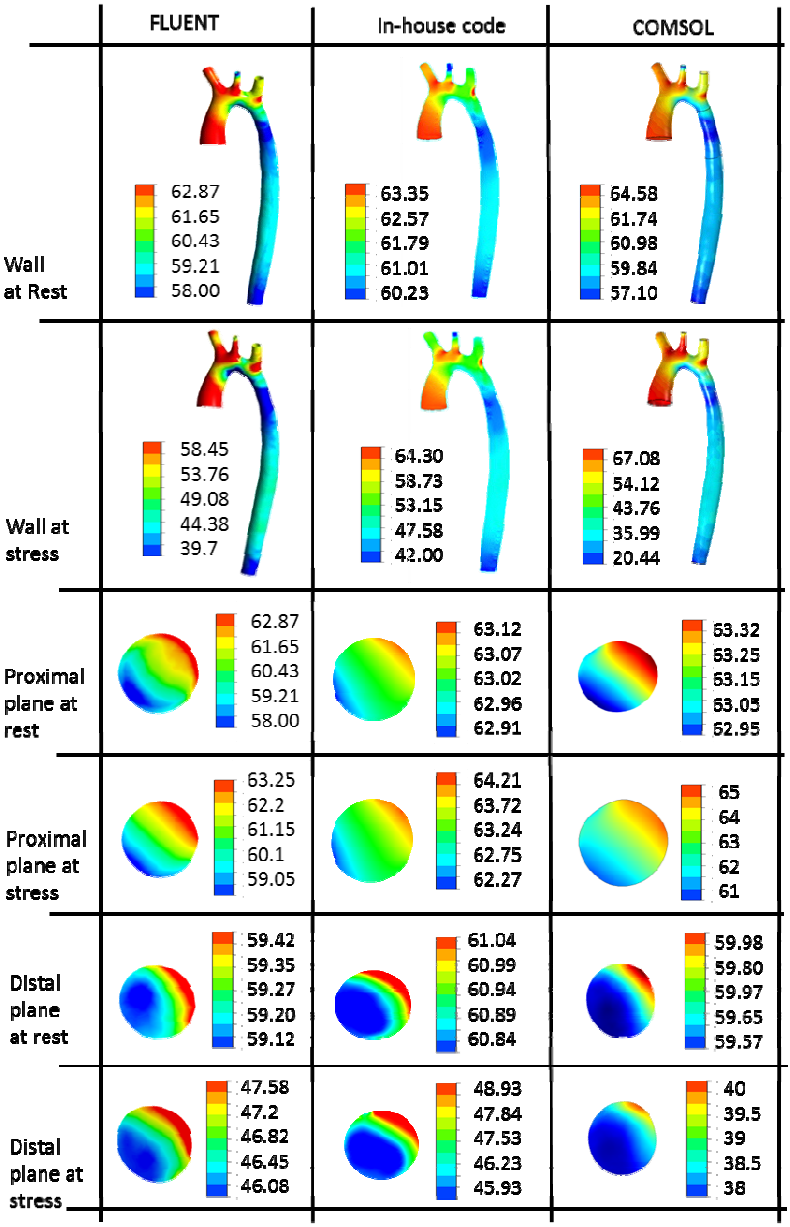

Fig. 4. Pressure gradients as observed at the wall, proximal and distal planes for FLUENT, in-house code and COMSOL

Table 3. Maximum, minimum and mean pressure at inlet and Dao including pressure drop (dP) across proximal and distal plane in mmHg

		Rest			Stress		
		FLUENT	In-house	COMSOL	FLUENT	In-house	COMSOL
Systole	Inlet	83.92	83.92	83.92	123.35	123.35	123.35
	Proximal (P)	81.46	83.06	82.91	111.16	118.50	116.03
	Distal (D)	68.13	66.92	68.33	70.52	51.84	26.33
	DAo	59.83	61.80	65.00	34.20	28.10	3.892
	dP = P – D	13.34	16.15	14.58	40.64	66.66	89.7
Diastole	Inlet	49.68	49.68	49.68	36.77	36.77	36.77
	Proximal	49.67	50.07	49.68	36.87	37.00	36.68
	Distal	49.48	49.99	49.68	39.07	37.36	36.63
	DAo	49.38	49.78	49.69	39.38	37.46	36.59
	dP = P – D	0.19	0.08	0.00	-2.20	-0.36	0.05
Mean flow	Inlet	63.35	63.35	63.35	64.30	64.30	64.30
	Proximal	62.96	63.02	63.12	61.34	63.24	62.34
	Distal	60.12	60.94	59.66	46.70	47.53	38.29
	DAo	58.55	60.23	58.64	35.52	42.01	32.22
	dP = P – D	2.84	2.08	3.46	14.64	15.71	24.04

In order to compare the nature of vortical structures in the DAo flow field between rest and stress conditions, helicity was computed as a flow derived parameter and rendered as isocontours (Fig 5a) for time-averaged inflow conditions. Helicity was computed as the normalized magnitude of the dot product between vorticity and velocity vectors at each node in the computed flow field. Positive helicity (highlighted red) indicates right handed vortical structures and negative helicity (highlighted blue) indicates left handed vortical structures. It was observed that opposing vortical structures are created as the flow enters the coarctation in a very similar formation for both rest and stress conditions in case of mild CoA. This was distinct from the opposing vortical structures that are formed which naturally spiral helically in the DAo by virtue of the curvature of the transverse aortic arch. However, the vortical structures distal to the modeled mild CoA were not as pronounced as seen for more severe CoA cases previously reported to demonstrate distinct downstream jet-flow effects[8].

Similar max-normalized cross-sectional velocity flow profiles were observed for the rest and stress conditions at the studied proximal and distal planes (Fig 5b) at rest and stress conditions. A shift in flow streams toward the outer curvature of the aortic arch was observed for stress conditions (viz. higher flow rates), leading to an elongated low-pressure pressure region distal to the CoA in contrast with the rest case (Fig 5b). Comparatively higher pressures were observed at the outer curvature of the aortic arch as seen on the proximal and distal plane (see Fig 4).

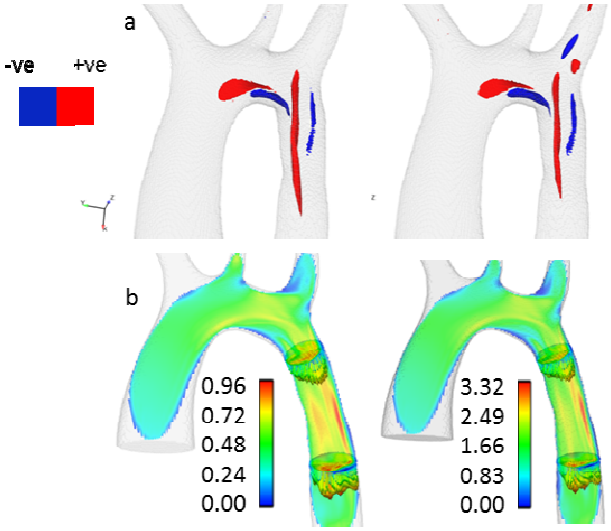

Fig. 5. Helicity isocontours (a) and velocity profiles (in m/s) (b) computed at mean pressures for rest (left) and stress (right) conditions

Pressure gradient across the CoA from the windkessel model showed transient variation at the peak systolic instant as an effect of factoring in compliance at the DAo as compared with the rigid wall simulations. Further, overall pressure values throughout the aorta model were found to increase significantly despite the mean pressure gradient not being affected considerably. This is congruent with the nature of the windkessel model for the cycle average pressure gradient calculation; as $dP_i/dt = 0$ and $dQ_i/dt = 0$ in equation (1) for the cycle average, which therefore reduces the equation to $P_i/Q_i = (R_1+R_2)$, therefore indicating that the pressure gradient should match that obtained for the cycle average obtained from rigid wall CFD simulations not factoring compliance. Fully coupled fluid structure interaction (FSI) methods can better predict clinically significant parameters such as pressure gradients for mean flows and wall shear stress for the arterial model as it considers the elastic properties of the arterial wall[18], while the windkessel approach still allows a tunable parameter to match physiological observations.

4 Conclusion

CFD is a powerful tool for simulation of altered hemodynamics in pathological anatomies and is investigated in this study as a diagnostic aid for evaluating pressure gradients across a patient-specific mild CoA. The downstream hemodynamics observed in the DAo was similar when simulated in three different rigid walls CFD solvers modeling viscous, incompressible blood flow, which in-turn were significantly different than pressure gradients computed from merely the inviscid Bernoulli formulation. However the rigid wall CFD approach is limited in the sense that regional

vascular wall-compliance requires to be considered accurately in order to yield physiologically relevant results. Compliances applied at the outlets may not be enough for accurate pressure predictions and hence FSI must be adopted in future to take into consideration regional elasticity of arterial walls in a manner matched to wall motion observable from gated cine cardiac MRI studies.

Acknowledgements. We acknowledge funding from the Pittsburgh Supercomputing Center (research allocation BCS120006) for facilitating the parallel CFD simulations presented in this work.

References

1. Mullen, M.J.: Coarctation of the aorta in adults: do we need surgeons? Heart 89, 3–5 (2003)
2. Habib, W.K., Nanson, E.M.: The causes of hypertension in coarctation of the aorta. Annals of Surgery 168, 771–778 (1968)
3. Garne, E., Stoll, C., Clementi, M., Euroscan, G.: Evaluation of prenatal diagnosis of congenital heart diseases by ultrasound: experience from 20 European registries. Ultrasound in Obstetrics & Gynecology: The Official Journal of the International Society of Ultrasound in Obstetrics and Gynecology 17, 386–391 (2001)
4. Russo, V., Renzulli, M., La Palombara, C., Fattori, R.: Congenital diseases of the thoracic aorta. Role of MRI and MRA. European Radiology 16, 676–684 (2006)
5. Valverde, I., Staicu, C., Grotenhuis, H., Marzo, A., Rhode, K., Shi, Y., Brown, A.G., Tzifa, A., Hussain, T., Greil, G., Lawford, P., Razavi, R., Hose, R., Beerbaum, P.: Predicting hemodynamics in native and residual coarctation: preliminary results of a Rigid-Wall Computational-Fluid-Dynamics model (RW-CFD) validated against clinically invasive pressure measures at rest and during pharmacological stress. Poster Presentation at SCMR/Euro CMR Joint Scientific Sessions, February 3-6 (2011)
6. Varga, A., Kraft, G., Lakatos, F., Bigi, R., Paya, R., Picano, E.: Complications during pharmacological stress echocardiography: a video-case series. Cardiovascular Ultrasound 3, 25 (2005)
7. Mertes, H., Sawada, S.G., Ryan, T., Segar, D.S., Kovacs, R., Foltz, J., Feigenbaum, H.: Symptoms, adverse effects, and complications associated with dobutamine stress echocardiography. Experience in 1118 patients. Circulation 88, 15–19 (1993)
8. Menon, P.G., Pekkan, K., Madan, S.: Quantitative Hemodynamic Evaluation in Children with Coarctation of Aorta: Phase Contrast Cardiovascular MRI versus Computational Fluid Dynamics. In: Camara, O., Mansi, T., Pop, M., Rhode, K., Sermesant, M., Young, A. (eds.) STACOM 2012. LNCS, vol. 7746, pp. 9–16. Springer, Heidelberg (2013)
9. Eli Konen, N.M., Provost, Y., McLaughlin, P.R., Crossin, J., Paul, N.S.: Coarctation of the Aorta Before and After Correction: The Role of Cardiovascular MRI. American Journal of Roentgenology 182, 1333–1339 (2004)
10. Rannacher, R.: Finite Element Methods for the Incompressible Navier-S tokes Equations. Advances in Mathematical Fluid Mechanics, 191–293 (2000)
11. Chung, T.J.: Transitions and interactions of inviscid/viscous, compressible/incompressible and laminar/turbulent flows. International Journal for Numerical Methods in Fluids 31 (1999)

12. Wesseling, P., S.A., Vankan, J., Oosterlee, C. W., Kassels, C.G. M.: Finite discretization of the incompressible Navier-Stokes equations in general coordinates on staggered grids. Presented at the 4th International Symposium on Computational Fluid Dynamics, Davis, CA (September 1991)
13. Neal, T., Frink, S.Z.P.: Tetrahedral finite-volume solutions to the Navier-Stokes equations on complex configurations. International Journal for Numerical Methods in Fluids 31, 175-187
14. Menon, P.G., Yoshida, M., Pekkan, K.: Presurgical evaluation of fontan connection options for patients with apicocaval juxtaposition using computational fluid dynamics. Artificial organs 37, E1–E8 (2013)
15. Yoshida, M., Menon, P.G., Chrysostomou, C., Pekkan, K., Wearden, P.D., Oshima, Y., Okita, Y., Morell, V.O.: Total cavopulmonary connection in patients with apicocaval juxtaposition: optimal conduit route using preoperative angiogram and flow simulation. European Journal of Cardio-thoracic Surgery: Official Journal of the European Association for Cardio-thoracic Surgery 44, e46–e52 (2013)
16. Westerhof, N., Lankhaar, J.W., Westerhof, B.E.: The arterial Windkessel. Medical & Biological Engineering & Computing 47, 131–141 (2009)
17. Cappello, A., Gnudi, G., Lamberti, C.: Identification of the three-element windkessel model incorporating a pressure-dependent compliance. Annals of Biomedical Engineering 23, 164–177 (1995)
18. Reymond, P., Crosetto, P., Deparis, S., Quarteroni, A., Stergiopulos, N.: Physiological simulation of blood flow in the aorta: Comparison of hemodynamic indices as predicted by 3-D FSI, 3-D rigid wall and 1-D models. Medical Engineering & Physics 35, 784–791 (2013)